Rarefaction after fast laser heating of a thin metal film on a glass mount

N. A. Inogamov, V. A. Khokhov, Y. V. Petrov, V. V. Zhakhovsky, K. P. Migdal, D. K. Ilnitsky, N. Hasegawa, M. Nishikino, M. Yamagiwa, M. Ishino, T. Kawachi, A. Y. Faenov, T. A. Pikuz, M. Baba, Y. Minami, and T. Suemoto

Citation: **1793**, 070012 (2017); doi: 10.1063/1.4971600
View online: http://dx.doi.org/10.1063/1.4971600
View Table of Contents: http://aip.scitation.org/toc/apc/1793/1
Published by the American Institute of Physics

RIGHTSLINK

Rarefaction after fast laser heating of a thin metal film on a glass mount

N.A. Inogamov[1,2,a)], V.A. Khokhov[1], Y.V. Petrov[1,3], V.V. Zhakhovsky[2], K.P. Migdal[2], D.K. Ilnitsky[2], N. Hasegawa[4], M. Nishikino[4], M. Yamagiwa[4], M. Ishino[4], T. Kawachi[4], A.Y. Faenov[5], T.A. Pikuz[6], M. Baba[7], Y. Minami[7] and T. Suemoto[7]

[1]*Landau Institute for Theoretical Physics, Russian Academy of Sciences, Chernogolovka, Russia*
[2]*Dukhov Research Institute of Automatics (VNIIA), Moscow, Russia*
[3]*Moscow Institute of Physics and Technology, Dolgoprudny, Russia*
[4]*Quantum Beam Science Center, Japan Atomic Energy Agency, Japan*
[5]*Institute for Academic Initiatives, Osaka University, Suita, Osaka, Japan*
[6]*Graduate School of Engineering, Osaka University, Suita, Osaka, Japan*
[7]*Institute of Solid State Physics, University of Tokyo, Tokyo, Japan*

[a)]Corresponding author: nailinogamov@gmail.com

Abstract. Understanding the physics of laser-matter interactions in ultrashort pulses is important for many well-acknowledged applications from material modifications to biology. We numerically and experimentally consider the effect of sub-picosecond Ti:sapp laser actions on 60-100 nm gold films mounted onto a fused silica substrate. The pulse energy is sufficient to ablate the films. For the first time, we show that there are different regimes of ablation, and the formation of the 3D structures depends on the value of the absorbed fluence F_{abs} and the adhesion strength p_{adh} between the film and the substrate. Namely, a delamination threshold F_{delam} and an ablation threshold F_{abl} ($F_{delam} < F_{abl}$) exist if adhesion is weak. Above the lower threshold F_{delam}, the whole film delaminates from the substrate. Above the higher threshold F_{abl}, the thin film ruptures near its middle plane. The external half of the film flies away, while the internal half remains on the glass substrate. There are two thresholds F_{delam} and F_{abl} for the Au/glass and Ag/glass targets, because pure gold and silver are weakly coupled to the glass. The lower threshold F_{delam} disappears in the case of a strong adhesion stress p_{adh}. Consequently, delamination as a whole becomes impossible. Although the rupture of a film remains because the ablation threshold F_{abl} is independent of on adhesion. Adhesion is high when an intermediate thin layer of chromium is placed between the gold and the glass. The film velocity after it separates from the substrate is low for the range of fluences $F_{delam} < F < F_{abl}$ because the acoustic impedance Z_{glass} of glass is small relative to the impedance Z_{film} of a gold film. Therefore, during an evolution, the absolute values (positive or negative) of the contact pressures are few times smaller than the absolute pressures in a gold film. However, above the ablation threshold $F_{abl} < F$, the velocity of the external part of a film becomes few times larger because the velocity is independent of the acoustic impedance of a substrate. These circumstances explain why 3D structures such as nanojet above the microbump appears in the case of a weak adhesion. The velocity should be not too large to allow to the surface tension and crystallization to stop an inflation and breakaway of a microbump.

INTRODUCTION

Localized solitary microstructures like microbumps, microholes, nanojets, and microcrowns are created by femtosecond (fs) and nanosecond (ns) laser pulses for important applications such as laser induced forward transfers, SERS, or fabrication of nanoscale plasmonic devices [1, 2, 3, 4, 5, 6, 7, 8, 9, 10]. Here we consider the action of ultrashort pulses with durations from few femtosecond to few picosecond. Number of experimental works increases fast, see the references given in the papers [4, 5, 6, 7]. The theory of the solitary microstructures was recently developed [9, 10]. It has been shown an irradiated film in the form of a flying cupola can tear away from the substrate [9, 10].

The motion of the cupola ends in either returning the delaminated film back to the substrate, or freezing of the cupola having with a parabolic or conical shape without a jet on the top, or forming a frozen cupola with a jet or a

Shock Compression of Condensed Matter - 2015
AIP Conf. Proc. 1793, 070012-1–070012-7; doi: 10.1063/1.4971600
Published by AIP Publishing. 978-0-7354-1457-0/$30.00

RIGHTSLINK

hole on the top. These scenarios are determined by a combination of four factors:

1. Melting of the film within an irradiated spot;
2. Tearing of a molten film from the substrate and formation of a flying cupola;
3. Mass flow to the top of cupola generated by the capillary deceleration and focusing to the axis;
4. Hardening of the cupola due to cooling followed by recrystallization in flight.

Previously the case with (i) a small adhesion stress p_{adh} and (ii) a tight focusing when the radius R_L of an illuminated spot is defined by the diffraction limit $R_L \sim \lambda$ has been considered [9, 10], where λ is the wavelength of an electromagnetic wave. In this case, below the ablation limit $F < F_{abl}$, both the velocity of a delaminated film $v \sim v_\sigma$, and the size R_L of a spot are small. Therefore, the capillarity becomes dynamically important when the separated film height rises above the substrate on the order $\sim R_L$, where $v_\sigma = 2\sqrt{\sigma/\mu_0}$ is the capillary velocity scale, σ is the coefficient of the surface tension, $\mu_0 = \rho_0 h_0$ is the initial surface density, and ρ_0 and h_0 are the initial room temperature density and film thickness,respectively.

Here we extend the results of these papers. First, the real electron heat conduction cooling of gold is included into our molecular dynamics (MD) simulations. Second, we consider the transition from small to large spots $R_L \gg \lambda$; wavelength $\lambda \sim 1$ μm for optical lasers. Third, we study the case of large adhesion when the film only partially separates from a substrate. It seems, that the case of large adhesion resembles partially the case of bulk targets. But there are qualitative differences. The ratio Z_{film}/Z_{glass} of acoustic impedances is large. This circumstance decreases an amplitude of tensile stress in the substrate and prevents rupturing inside the substrate with a rather large material strength. Unlike the bulk case, the depth where nucleation occurs for the fluence near the ablation threshold is defined by the film thickness d_f and not the thickness d_T of a heat affected layer in a bulk target; of course, we consider the case of a thin film where $d_f < d_T$. The case with a large ratio $Z_{film}/Z_{glass} \gg 1$ is similar to the case of a freestanding film [11].

We determine a way to simulate large objects [2 μm $\times$ 2 μm $\times$ (0.1+0.3) μm containing $\sim 100 \cdot 10^9$ atoms] using much smaller ones (containing $\sim 0.01 \cdot 10^9$ atoms) by MD. Typical experiments employ large objects [1, 2, 3, 4, 5, 6, 7, 8]. Here the film thickness is 0.1 μm, while the glass layer thickness, which influences the film dynamics during delamination, is 0.3 μm. Recall that a deficit of computer resources for description of a real situation is the commonly encountered problem in the MD simulations. In our approach, the approximately equivalent miniature systems have an order of magnitude smaller spatial scales and their evolutions up to freezing are an order of magnitude shorter. This is the main achievement of the paper, which is based on double scaling using, firstly, a capillary scale and, secondly, a thermal scale, as shown below. Thus, the large and small systems are equivalent in the sense that they have equal capillary and thermal numbers. We vary the film velocity after delamination and the heat conduction coefficient to achieve those equalities for different sized systems.

SMALL SPOT, WEAK ADHESION

We separate the early stage $t \sim t_s = d_f/c_s \sim 20$ ps and the later stage $t \sim R_L/v \sim 10$ ns similar to [9, 10], where c_s is the speed of sound and v is the local velocity of the center of mass of a film after its delamination. This separation of the stages greatly simplifies the problem because only the 1D dynamic influence of the glass substrate onto motion of a film has to be considered (i.e., only during the early stage the substrate is presented). Therefore the MD run of the later stage covers only matter of a film.

In the range $F_{delam} < F < F_{abl}$, the film separates as a whole from the substrate. Figure 1(a) shows the dependencies $v(F)$ for three different values of the adhesion strength p_{adh}. Figure 1(a) demonstrates that the range occupied by the delamination regime gradually decreases as the adhesion p_{adh} becomes stronger and finally disappears above a certain limit for p_{adh}.

The points m_b and m_f in Figure 1(a) denote the range of fluences where the volume fraction of molten gold appears (above m_b) and the whole film is molten (above m_f). The temperature distribution for thin films is approximately homogeneous across film thickness. Therefore, the film is a solid-liquid mixture between the points $m_b - m_f$.

The ratio of the film thickness to the diameter ($d_f \sim 0.1$ μm, $2R_L \sim 1$ μm) is small even for a small spot. Therefore, the hydrodynamic velocities at the early stage are directed mainly along the normal direction relative to the film (Fig. 1(b)). In our approach, the early stage is simulated by a 1D two-temperature (2T) hydrodynamic code (1D 2T-HD), including full 2T physics [12]. The 2T-HD results for the local velocity of a center of mass of a local small piece of a film are shown in Fig. 1(c).

RIGHTSLINK

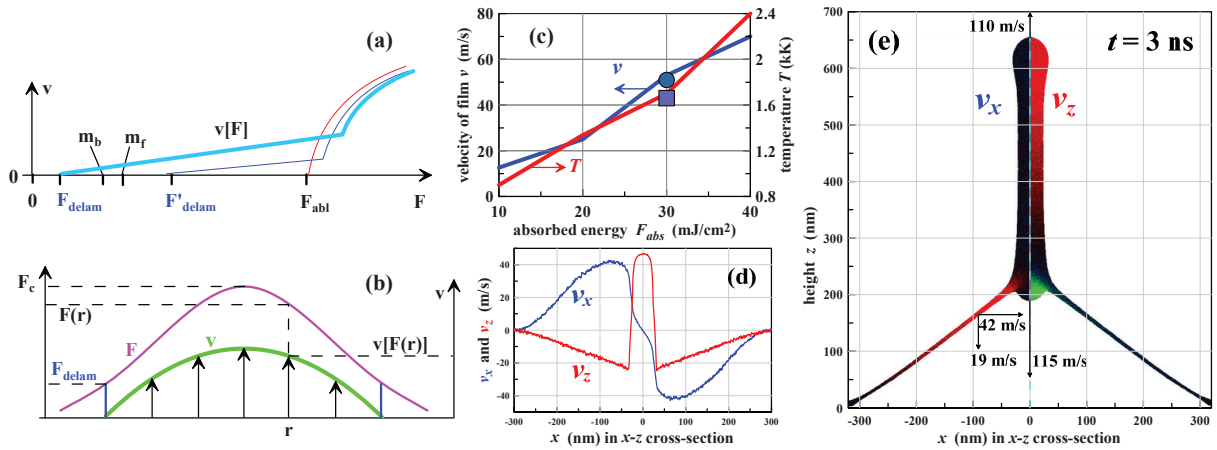

FIGURE 1. (a) Schematic presentation of the dependence of the film velocity (velocity after separation of the film) from a local fluence. Weak adhesion has two thresholds and three regimes separated by the two thresholds, but the intermediate regime ($F_{delam} < F < F_{abl}$) disappears in the case of strong adhesion. (b) Fluence distribution $F(r)$ across the illuminated spot and the corresponding velocity distribution $v[F(r)]$; F_c is the maximum fluence. (c) Dependencies of the recoil velocity and average temperature T on absorbed energy F_{abs} for a gold film $d_f = 60$ nm. These values are obtained after separating the film from the glass substrate. Melting temperature of gold is 1.337 kK. Circle and square correspond to the case where the adhesion strength of the Au/glass contact $p_{adh} = -1$ GPa and $p_{adh} = -2$ GPa, respectively. They are blue corresponding to the velocity dependencies. Curves show the case $p_{adh} = 0$. (d) Components of the velocity in the flying cupola according to the MD simulation. Normal and tangential components relative to the plane of a target are shown. Profiles are obtained by averaging the particle velocities within the thin vertical x-slabs along z-axis. We see that *in average* (there are small part going down) matter of the jet is going up, while the shell begins its return back to the substrate. Directions of the horizontal velocities obviously show how the shell feeds the jet. (e) Velocity field in the flying cupola with outward and inward jets obtained in the MD simulation at $t = 3$ ns. Arrows show the directions of velocity in the corresponding points (the lengths of the arrows in different points are not in scale). (Left part) Map of the horizontal v_x component of the velocity. This component is tangential relative to the substrate surface. Light red shows particles with a high positive velocity. Darker colors correspond to smaller v_x. (Right part) Colors correspond to the vertical (normal to the substrate surface) component of velocity v_z, where red and green denote particles going up and down, respectively.

The range of absorbed energies F_{abs} in Fig. 1(c) is within the range $F_{delam} < F < F_{abl}$ shown in Fig. 1(a). The influence of the adhesion strength p_{adh} is illustrated by the small circle and the small square in Fig. 1(c). In Fig. 1(a), the delamination threshold F_{delam} corresponds to the smallest strength p_{adh}. The delamination threshold F'_{delam} in Fig. 1(a) is higher than F_{delam} because it corresponds to a larger adhesion. The ablation threshold F_{abl} (see Fig. 1(a)) weakly depends on the adhesion if the difference in the acoustic impedances is large. There is a value of the strength p_{adh} for which the threshold F_{delam} increases up to the ablation threshold F_{abl}. For systems with this or stronger adhesion, the regime where a film delaminates as whole from a substrate disappears.

The velocity distribution from Fig. 1(b) serves as the initial velocity distribution for the later stage of the problem; the later stage begins when the piece of a film separates from the substrate. It is clear that the inhomogeneous velocity distribution from Fig. 1(b) results in the cupola-like convex shape of the growing microbump. The rising bump follows the spatial distribution of the fluence $F(r)$ (e.g., if there is a well in the distribution $F(r)$, then a well appears in the shape of a bump).

The later stage (from the delamination instant to infinity) is simulated by MD. Figures 1(d,e) and 2(a) illustrate the interplay between the normal component of momentum of the film and the capillary stresses. The normal component of a momentum is accumulated by the film during the delamination process (i.e. in the early stage). This can also be called a recoil process since the film undergoes a thermomechanical recoil from the substrate after laser impact. The recoil momentum is accumulated due to pressure acting from a glass side through the Au/glass contact onto the gold film. The capillary stress acts against the normal momentum decreasing its value by transferring momentum from the flying part of the film to the remnant part of the film and to the massive substrate. The transfer is implemented along the film and the circle of contact where the flying part of a film joins the remnant of the film.

The surface energy increases as the surface area increases. Therefore, without breaking the flying film or jet and/or without freezing the liquid back into solid state, the surface tension inevitably returns all the delaminated mass

RIGHTSLINK

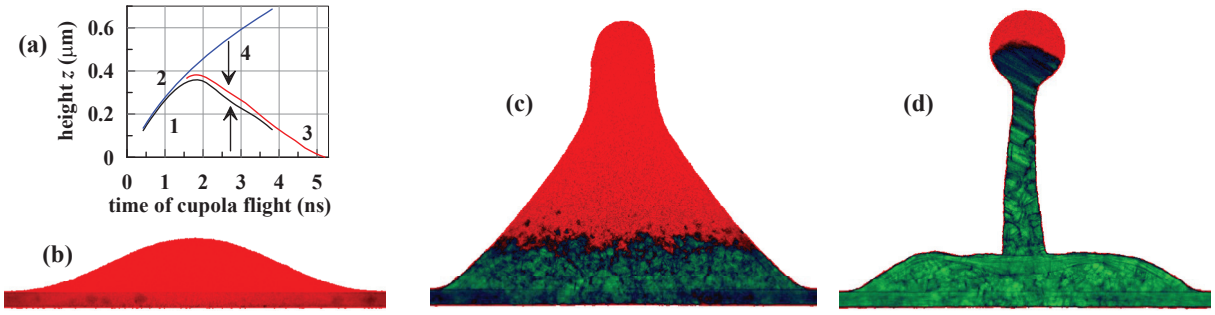

FIGURE 2. (a) Trajectory 1 is the trajectory of the apex point of the bottom surface of the cupola shell. This point belongs to the z-axis and to the bottom surface. After formation of the counter-jet, this is the tip or apex point of the counter-jet. Point 2 corresponds to the upper apex, which is the point where the z-axis intersects the upper surface of a bump and jet. Again, after formation of the jet, this is the apex of the jet. Point 3 is where the cupola shell attaches (or transfers) to the axial jet structure. It begins to differ from point 1 when the counter (or inverse) jet appears. Similarly point 2 begins to stand significantly above the shell when the direct jet begins to grow. Arrows 4 shows the height of the inverse jet. The description corresponds to Fig. 1(e,d) with a negligible crystallization velocity. In this case, the skirt of the conically shaped nanobump returns back to the substrate surface, see curve 3. (b), (c), (d) Competition between the capillary deceleration and crystallization. Red and green correspond to molten and solid gold, respectively. This is the case when the recrystallization speed is sufficiently fast. Therefore the nanobump solidifies before it touches the substrate.

back onto substrate. This easily explains the appearance of debris in the form of nanodroplets at the target's surface after laser irradiation. (See also [9], which shows how the droplets return back to the target.) Questions about the decay of the jet into droplets and the rupture spots of the film, which form the surface of the cupola, will be described elsewhere. However, freezing and recrystallization are considered below.

Let us try to explain (in simple words) why the jet appears. This is a result of counteraction between, firstly, surface tension and, secondly, inertia. Firstly, there are capillary bonds between the liquid particles. These bonds form the restoring force which tries to keep integrity of our liquid moving object (flying shell) and to return the object back to the substrate. But the object is a highly mobile fluid. There are a lot of degrees of freedom inside the multitude of liquid particles (forming the shell) even constrained by the capillary bonds.

Secondly, inertia. Fluid resists to the forcible return. It tries to keep its recoil momentum directed outward the substrate. Fluid uses its internal degrees of freedom to resist to the forcible return (return back onto the substrate). This is the reason why the jet is formed, see also explanations in [10]. The jet formation weakens the ties to the contact circle at the substrate for the mass particles in the jet (the contact circle of the cupola is the sink for the recoil momentum of the cupola). Thus the ratio between the inertial and capillary stresses is larger for the particles in the jet relative to the particles in the film. Nevertheless, the permanently acting surface tension will finally stop and return the jet. The only ways to avoid this are: the Plateau–Rayleigh instability or freezing.

The capillary focusing causes the radial mass flux to converge to the axis (the velocity directions in Figs. 1(d,e)). In turn, the convergence causes a collision with the axis and the formation of a jet and an opposite jet or counter-jet ([10] and Fig. 7 in [2]). The jets formation starts after the instant when the motion of the upper part of the bump shell stops and reverses. These behaviors along with the trajectories of the jet and counter-jet tips are shown in Fig. 2(a). Thanks to the curved bump and the return motion of the bump, which is obvious from the instant velocity distributions shown in Figs. 1(d,e), the jet and the counter-jet are not equivalent. After the bump stops, the upper part of the bump shell moves down in Fig. 1(e), increasing the length of the jet while decreasing the length of the counter-jet.

Cooling and solidification prevent the complete return of the delaminated mass. Cooling is due to the conductive spread of the thermal energy from a hot spot to the cold film around the hot spot. We neglect a heat conductivity of a glass. This cooling is unimportant for the motion of a film as long as gold remains molten because the surface tension $\sigma(T)$ weakly depends on the temperature within our temperature range. However, freezing changes the situation qualitatively because frozen gold loses its stretching ability. This circumstance sharply but not immediately reduces the velocity of the frozen parts of a cupola by a fast transfer of momentum of frozen mass to the contact circle (Figs. 2(c) and (d)). Below the bending of the walls of the solid thin shell and the formation of multiple folds on the surface

RIGHTSLINK

of a bump are discussed.

Our MD code, which is used to simulate the evolution of a film after detachment, has an important advantage. It contains a Monte-Carlo addition, which describes the electron heat conductivity. The conductivity value depends on the frequency of the electron jumps from one atom to its neighbor. Thus, it is possible to regulate the heat conduction coefficient κ. This ability can be employed to adjust the necessary value of heat conduction. For MD simulations, the EAM potential of gold developed in paper [13] is used.

The double scaling allowed us to decrease the computer resources necessary for the simulation. There are three main velocities in the problem: (a) velocity v_0 in the center of a cupola after separation of the film, (b) the introduced capillary velocity $v_\sigma = 2\sqrt{\sigma/\mu_0}$, and (c) the thermal velocity $v_\chi = \chi/(2R_L)$. Here $\chi = \kappa/c$ is the heat diffusivity and c is the heat capacity. This means that there are two non-dimensional scaling parameters v_σ/v_0 and v_χ/v_0. The problems with the large and small hot spots are equivalent if they have the same parameters. Thus, we chose a smaller radius R_L in the simulation and adjusted the velocity v_0 and the conductivity κ in the simulation so that the two scaling parameters in the simulation are the same as the experiments. The parameters in the simulation shown in Figs. 2(b-d) are $v_0 = 385$ m/s, $v_\sigma = 150m/s$, $v_\chi = 66$ m/s; corresponding scaling parameters are $v_\sigma/v_0 = 0.4$ and $v_\chi/v_0 = 0.2$.. Typical velocities and scaling parameters in experiments [1, 2, 3, 4, 5, 6, 7, 8] are $v_0 = 100 - 150$ m/s, $v_\sigma = 60$ m/s, $v_\chi = 50$ m/s, $v_\sigma/v_0 = 0.6 - 0.4$, and $v_\chi/v_0 = 0.5 - 0.3$. Comparing the simulations in Figs. 2(b-d) and the experiments, we can conclude that the simulation satisfactorily describes the experiments.

The bumps shown in Fig. 1(e) and Figs. 2(b-d) transit during their evolution from a parabolic to a conical shape near the stopping point (Fig. 1(e)). The height of the conical skirt decreases after the stopping point (Figs. 2(c,d)). There is some amount of kinetic energy connected with the velocities of this decrease. Therefore, the skirt cannot be stopped immediately after solidification. It continues its fall to the substrate. Because the average area of the solidified skirt decreases during the fall, multiple folds or multiple radial ripples form on the skirt's surface where the excess of the solid surface is stored. References [2, 8] show experimental examples of such folds.

It should be mentioned that the signal from the ruptured small spot at the bump surface expands with a rather limited (for our range of film thicknesses) velocity $v_\sigma/\sqrt{2}$, see expression (31) in [10]. This velocity is on the order or smaller than the velocity of the crystallization front and the velocity of the bump motion. Thus, even a bump with a perforating spot may follow its evolution up to contraction and solidification. Reference [2] provides an example (see Fig. 7 in [2]). The dynamics of the hole's expansion along a membrane is considered in [10, 14].

LARGE SPOT, STRONG ADHESION

As previously mentioned, the delamination range in Fig. 1(a) shrinks and disappears as the contact adhesion p_{adh} increases. For a large ratio of acoustic impedances (e.g., gold on glass), the absolute values of the positive and negative pressures at a contact are several times smaller than the absolute pressures inside a film. (See Fig. 3(a) in [15].) Firstly, the velocity increases at the point F_{abl} in Fig. 1(a) for any adhesion. Secondly, the limiting contact adhesion $p_{adh}|_{lim}$ (when the delamination disappears) is several times smaller than the material strength of gold. Namely, this velocity jump in the point F_{abl} in Fig. 1(a) makes it difficult to form a frozen cupola for $R_L \sim 1$ μm because the surface tension is weak against the high velocity and cannot prevent the breakaway of a cupola. An interesting but unstudied situation appears if the thresholds F_{delam} and F_{abl} shown in Fig. 1(a) coexist and the central fluence F_c defined in Fig. 1(b) overcomes F_{abl}. Figure 3 shows the case of strong adhesion $p_{adh} > p_{adh}|_{lim}$.

The nucleation shown in Fig. 3(a) begins inside the gold film. The upper layer flies up forming a convex shell (cupola or dome). The cupola inflates and is seen even at very late stages (hundreds ns) when its height h_{cup} above the substrate plane is equal to several diameters $2R_L \approx 100$ μm of a large irradiated spot, which requires a separate description. A comparison of the initial kinetic energy $\mu_0 v^2/2$ and the surface energy 2σ gives the capillary scale $v_\sigma = 2\sqrt{\sigma/\mu_0}$. However, the radius R_L is absent in the expression for the capillary velocity v_σ, although the radius R_L defines the curvature of a cupola at the height $h_{cup} \sim 2R_L$. The velocity dh_{cup}/dt of a cupola loses one capillary unit of velocity when it passes up one spatial unit $2R_L$. This is the surface tension deceleration of flight for any spot from small to large.

The absence of R_L in the scale v_σ makes the situation universal and independent of the value of the radius R_L as long as a cupola maintains its integrity. Thus, the simulation without Monte-Carlo heat conduction shown in Fig. 1(e) for $2R_L \sim 1$ μm is also valid for large R_L. This is true until the cooling is insignificant $v_\chi \ll v_\sigma$. For a large R_L, the role of solidification is small because the velocity $v_\chi = \chi/(2R_L)$ is small. Therefore, the solidification begins late. The solidification defines the frozen edges, which form a very high ring around the crater in Fig. 3(b) obtained

RIGHTSLINK

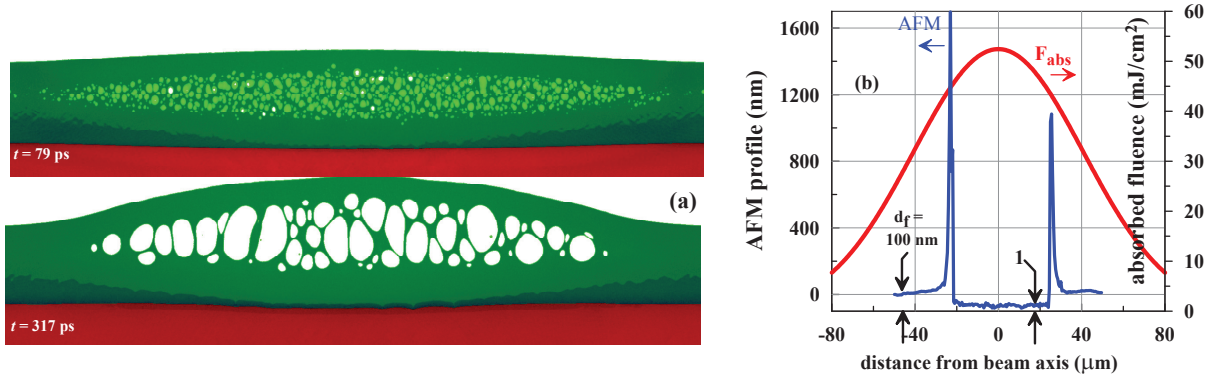

FIGURE 3. (a) MD simulation of the internal rupture of a 100-nm-thick gold film in the case with a large adhesion to the glass substrate. (b) Final shape of the rim and the crater after separation of the overinflated cupola from the remnant of the film [16]. It is likely that the separation occurs at the dividing line between the crystallization front and the molten gold, where the stretchability jumps. See [4] where the neck between the solid and the liquid parts is observed. Arrow 1 denotes the remnant film remaining on the substrate after laser action.

in experiments [16, 17, 18] with a Ti:sapp laser acting on the 100-nm-thick gold film with 20-nm-thick chromium underlayer on a glass substrate.

DISCUSSION AND CONCLUSIONS

To conclude, it is worth mentioning that the above interplay between the recoil of the film, adhesion, surface tension, cooling/solidification, and lateral sizes of spots is considered. This interplay in the limited parameter space (double scaling) results in various behaviors.

Additional studies are in development. They will describe the shortcomings and limitations of the double scaling. The lifetime τ_{mtstb} of a metastable stretched liquid exponentially depends on the amplitude of the tensile stress p and the temperature T : $\tau_{mtstb} = A\exp(-U/T)$, $U = (16\pi/3)\sigma^3/p^2$. Spatiotemporal scales influence the pre-exponential factor A. Thus, there is a weak (logarithmic) increase in the thresholds F_{delam}, F_{abl} for thinner films. This is one limitation. However, the film in Fig. 3(a) has a thickness equal to the experimental conditions, whereas those in Figs. 1(d,e) and Figs. 2(b-d) have a breakaway of the glass-gold contact (not bulk) for which we have crude estimates of the adhesion stress p_{adh}. The physics of delamination of molten gold from a substrate differs from the physics of nucleation in a bulk metastable stretched liquid.

A similar limitation is that for a smaller object, the faster the temperature decreases, the larger the degree of overcooling of the liquid during recrystallization. This also seems to be a weak shortcoming because the thermal velocities $v_\chi = 50 - 70$ differ moderately between the experimental conditions and the simulation using the double scaling. Velocities $v_\chi = 50 - 70$ m/s are on the order of the diffusion limited recrystallization velocity.

A more difficult problem is connected with the description of the breakaway of the stretched film as described in References [9, 10, 14]. Our simulations used films like the one shown in Figs. 2(b-d), which are 5-10 times thinner than those in the experiments with nanobumps [1, 2, 3, 4, 5, 6, 7, 8]. The breakaway of a film begins when a film is stretched to thicknesses $\sim 1 - 2$ nm. This conclusion follows from papers [9, 10, 14]. The physics to create valuable nuclei in the form of the puncture of a film due to thermal fluctuations is considered in [14]. The film is stretched two to three times during inflation of a cupola and the formation of a jet. This is insufficient for a thermo-fluctuational puncture even for the thin film shown in Figs. 2(b-d). Thus, our scenario shown in Figs. 2(b-d) is entirely adequate for the experiments [1, 2, 3, 4, 5, 6, 7, 8] (coincidence of the capillary and thermal scalings and absence of a puncture).

The question to be addressed in future works is how to rupture a $\sim$ 50-nm-thick film? Stretching 20-50 times requires the proportional expansion of the surface area. This seems to be too large for the homogeneous inflation of the bump. Thus, some local amplification of the stretching or the inhomogeneous expansion is necessary. This maybe the region between the molten and solidified film or, in the case of nucleation inside the middle plane of the film (shown in Fig.3a), the inhomogeneous traces of nucleation and foaming induce slightly different expansion velocities

RIGHTSLINK

of the inflating cupola. Finally, we should mention that the decay of the jet into droplets together with the running solidification of the jet is nicely described in our model. However, the corresponding pictures are beyond the scope of this short paper.

ACKNOWLEDGMENTS

The research (NAI, VVZh, VAKh, DKI, YVP, KPM, AYF, TAP) has been performed under financial support from Russian Science Foundation (RSCF) (project No. 14-19-01599).

REFERENCES

[1] F. Korte, J. Koch, and B. N. Chichkov, Appl. Phys. A **79**, p. 879 (2004)
[2] C. J. Koch,L. Overmeyer, and B. Chichkov, Optics Express **20**, p. 24864 (2012)
[3] Y. Nakata, T. Okada, and M. Maeda, Jpn. J. Appl. Phys. **42**, L1452 (2003)
[4] D. Ivanov, A. Kuznetsov, V. Lipp, B. Rethfeld, B. Chichkov, M. Garcia, and W. Schulz, Appl. Phys. A. **111**, p. 675–687 (2013)
[5] A. Kuchmizhak, A. Ionin, S. Kudryashov, S. Makarov, A. Rudenko, Y. Kulchin, O. Vitrik, and T. Efimov, Optics Letters **40**, p. 1687–1690 (2015)
[6] M. Domke, S. Rapp, and H. Huber, Physics Procedia **39**, p. 717–725 (2012)
[7] U. Zywietz, A. B. Evlyukhin, C. Reinhardt, and B. N. Chichkov, Nature Communications **5**, p. 3402 (2014)
[8] M. Armstrong, *The evolution of ultrafast compression*, SIMES Seminar, (2015) https://simes.stanford.edu/events/mike-armstrong-simes-seminar
[9] N. A. Inogamov and V. V. Zhakhovskii, JETP Letters **100**, p. 4–10 (2014)
[10] N. A. Inogamov, V. V. Zhakhovskii, and V. A. Khokhlov, JETP **120**, p. 15–48 (2015)
[11] A. K. Upadhyay, N. A. Inogamov, B. Rethfeld, H. M. Urbassek, Phys. Rev. B **78,** 045437 (10 pages) (2008).
[12] V. Khokhlov, N. Inogamov,V. Zhakhovsky, D. Ilnitsky, K. Migdal, and V. Shepelev, Film-substrate hydrodynamic interaction initiated by femtosecond laser irradiation, in *19th Biennial Conference of the APS Topical Group on Shock Compression of Condensed Matter*, Vol. 60 Bulletin of the American Physical Society, (2015) Abstract: W1.00047
[13] V. V. Zhakhovskii, N. A. Inogamov, Yu. V. Petrov, S. I. Ashitkov, and K. Nishihara, Applied Surface Science **255**, p. 9592–9596 (2009)
[14] N. A. Inogamov, V. V. Zhakhovsky, S. I. Ashitkov, Y. N. Emirov, A. Y. Faenov,T. A. Pikuz, M. Ishino, M. Kando, N. Hasegawa, M. Nishikino, T. Kawachi, M. B. Agranat, A. V. Andriash, S. E. Kuratov, and I. I. Oleynik, Journal of Physics: Conference Series **500**, 112070 (2014)
[15] N. Inogamov, V. Khokhlov, V. Zhakhovsky, Y. Petrov, K. Khishchenko, and S. Anisimov, *Femtosecond laser ablation of thin films on substrate,* in PIERS Proceed. (ISSN 1559-9450), Prague, Czech Republic, July 6-9, 2015, pp. 2422–2426 (2015). http://piers.org/piersproceedings/piers2015PragueProc.php?searchname=inogamov
[16] M. Nishikino, N. Hasegawa,T. Tomita, Y. Minami, R. Takei, M. Baba, T. Eyama, S. Takayoshi,T. Kawachi, D. Hatomi, N. Ohnishi, M. Yamagiwa, and T. Suemoto, Proc. SPIE **8849**, 88490E (2013)
[17] T. Tomita, M. Yamamoto,N. Hasegawa, K. Terakawa, Y. Minami, M. Nishikino, M. Ishino, T. Kaihori, Y. Ochi, T. Kawachi, M. Yamagiwa, and T. Suemoto, Optics Express **20**, p. 29329–29337 (2012)
[18] T. Tomita, M. Nishikino,N. Hasegawa, Y. Minami, R. Takei, M. Baba, T. Eyama, S. Takayoshi,T. Kaihori, T. Morita, Y. Hirano, T. Kawachi, M. Yamagiwa, and T. Suemoto, JLMN-Journal of Laser Micro/Nanoengineering **9**, p. 137–142 (2014)

RIGHTSLINK